











Experimental and Theoretical Insights on Chemopreventive Effect of the Liposomal Thymoquinone Against Benzo[*a*]pyrene-Induced Lung Cancer in Swiss Albino Mice

Arif Khan ¹, Mohammed A Alsahli ², Mohammad A Aljasir ², Hamzah Maswadeh ³,
Mugahid A Mobark ^{4,5}, Faizul Azam ⁶, Khaled S Allemailem ², Faris Alrumaihi ²,
Fahad A Alhumaydhi ², Ahmad A Almatroudi ², Naif AlSuhaymi⁷, Masood A Khan ¹

¹Department of Basic Health Sciences, College of Applied Medical Sciences, Qassim University, Buraydah, 51452, Saudi Arabia; ²Department of Medical Laboratories, College of Applied Medical Sciences, Qassim University, Buraydah, 51452, Saudi Arabia; ³Department of Pharmaceutics, College of Pharmacy, Qassim University, Buraydah, 51452, Saudi Arabia; ⁴Department of Pharmacy Practice, College of Pharmacy, Qassim University, Buraydah, 51452, Saudi Arabia; ⁵Department of Pathology, Faculty of Medicine, University of Kordofan, El-Obeid, Sudan; ⁶Department of Pharmaceutical Chemistry and Pharmacognosy, Unaizah College of Pharmacy, Qassim University, Unaizah, 51911, Saudi Arabia; ⁷Department of Emergency Medical Services, Faculty of Health Sciences, AlQunfudah, Umm Al-Qura University, Makkah, 21912, Saudi Arabia

Correspondence: Arif Khan, Department of Basic Health Sciences, College of Applied Medical Sciences, Qassim University, Buraydah, 51452, Saudi Arabia, Tel +966 590038460, Fax +966 63801628, Email 4140@qu.edu.sa

Purpose: Thymoquinone (TQ), a phytoconstituent of *Nigella sativa* seeds, has been studied extensively in various cancer models. However, TQ's limited water solubility restricts its therapeutic applicability. Our work aims to prepare the novel formulation of TQ and assess its chemopreventive potential in chemically induced lung cancer animal model.

Methods: The polyethylene glycol coated DOPE/CHEMS incorporating TQ-loaded pH-sensitive liposomes (TQPSL) were prepared and characterized. Mice were exposed to benzo[*a*]pyrene (BaP) thrice a week for 4 weeks to induce lung cancer. TQPSL was administered three times a week for 21 weeks, starting 2 weeks before the first dose of BaP.

Results: The prepared TQPSL revealed 85% entrapment efficiency with 128 nm size and -19.5 mV ζ -potential showing high stability of the formulation. The pretreatment of TQPSL showed the recovery in BaP-modulated relative organ weight of lungs, cancer marker enzymes, and antioxidant enzymes in the serum. The histopathological analysis of the tissues showed that TQPSL protected the malignancy in the lungs. The flow cytometry data revealed the induction of apoptosis and decreased intracellular ROS by TQPSL. Molecular docking was performed to predict the TQ's affinity for eight possible anticancer drug targets linked to lung cancer etiology. The data assisted to identify the serine/threonine-protein kinase BRAF as the most suitable target of TQ with binding energy -6.8 kcal/mol.

Conclusion: The current findings demonstrated the potential of TQPSL and its possible therapeutic targets of lung cancer. To our knowledge, this is the first research to outline the development of TQ formulation against lung cancer considering its low solubility as well as pulmonary delivery challenges.

Keywords: thymoquinone, pH-sensitive liposomes, lung cancer model, molecular docking

Introduction

According to GLOBOCAN 2020, the lung cancer is ranked second after the breast cancer in occurrence as 11.4% of total 18.1 million new cancer cases, while the breast cancer cases were recorded as 11.7%. However, the cancer-associated death in lung cancer was estimated to be first as 18% among 1.8 million mortalities from cancer.¹ As evident from several studies that the consumption of tobacco has the major role in the development of lung cancer as several fold increased were registered in the progression of the disease in smokers while comparing non-smokers.²⁻⁵ The benzo[*a*]pyrene (BaP) is the main carcinogen in the smoke of the cigarette, which may affect directly or indirectly, in the etiology

of lung cancer. The BaP is metabolically activated into 7,8-diol-9,10-epoxide and make the DNA adduct formation to initiate the cancer followed by promotion and progression. So, the BaP is the most appropriate carcinogen among polycyclic aromatic hydrocarbons, which has been utilized in all three stages of lung cancer in experimental animal models.^{6–8}

Several approaches have emerged to investigate the usefulness of natural dietary secondary metabolites in preventing and treating various illnesses, including cancer.^{9–11} Moreover, according to multiple epidemiological research, dietary habits may potentially have a role in the prevention and development of cancer and other illnesses.^{12–14} Evidently, the inclusion of some foods in the diet may decrease the risk of cancer, and 33% cancer associated death. Interestingly, the drug development data showed that approximately 50% of the drugs available in the market in last three decades were either directly derived from natural sources or chemically modified.^{14–18} Moreover, the use of drugs as herbal medicines from natural resources has been popular since ancient times across the world.

Thymoquinone (TQ) is a predominant secondary metabolite found in black seeds (*Nigella sativa*) that has been widely explored for its involvement in cancer prevention and development.^{19–21} The black seeds and its oil have been used in the cure of several infectious and non-infectious diseases in the various regions of the world.^{22,23} Evidently, TQ has been shown its potential in the treatment of various types of cancer through the activation of multiple signalling pathways that lead to the apoptosis.^{21,24,25} However, regardless of high potential, the major drawback of TQ is the low solubility in the aqueous solutions, which limits its uses in the clinical application. Thus, the preparation of suitable formulations of TQ can overcome this limitation to utilize its efficacy against several pathological conditions.^{26,27} Recently, we prepared the PEG-coated DSPC/Chol liposomes and demonstrated its stability and efficacy against A549 and H460 cancer lines. The TQ-liposomes also have been shown to minimize the toxicity in Swiss albino mice by *in vivo* acute toxicity assay.²⁸ Earlier, we reported the efficacy of TQ-entrapped liposomes against diabetes and various strains of *A. baumannii*- and *C. albicans*-infected animal models.^{29,30} Some researchers also showed the efficacy of TQ-liposomes against breast cancer cells *in vitro* and *in vivo* as well.^{31,32} However, the pulmonary delivery of TQ via oral gavage is the challenging task in the preparation of effective lipid-based formulation. The liposomal formulation of TQ must be protected from the hostile environment in order to avoid degradation in the gastrointestinal (GI) system. As evident from several research, sterically stabilized, small nano-sized, PEGylated liposomal formulations have proved their advancement in the lipid-based drug delivery vehicles. The addition of polyethylene glycol (PEG) in the liposomes protects it from the accessibility of enzymes due to its thick water.^{33–35} The long circulating stealth liposomes improve the extravasation in solid tumors due to vascular disruptions related to tumor angiogenesis.^{36–38} The PEGylated liposomes make no direct interaction with the target cancer cells while releasing the drug for eventual diffusion into them.^{39–42} Furthermore, it is known that tumor tissues have acidic condition as pH 5.0–6.5, in comparison to pH 7.4–7.5 in normal tissues. The pH-sensitive liposomes degrade and exhibit fusogenic characteristics, resulting in the release of their contents at slightly acidic pH. The preparation of pH-sensitive liposomes is able to deliver the drug into the cytoplasm of malignant cells.^{43,44} The current study attempts to develop and characterize pH-sensitive stealth liposomes, as well as to assess their chemopreventive potential *in vivo* in lung cancer models.

Methods

Materials

Dioleoylphosphatidylethanolamine (DOPE), cholesteryl hemisuccinate (CHEMS), 1,2-distearoyl-*sn*-glycero-3-phosphatidylethanol-amine-*N*-[methoxy(polyethylene glycol)-2000] (DSPE-PEG₂₀₀₀), were procured from Sigma-Aldrich (St. Louis, MO, USA). The benzo[a]pyrene (BaP), Annexin V-FITC/PI, DCFDA/H2DCFDA-Cellular ROS Assay kits, adenosine deaminase (ADA), lactate dehydrogenase (LDH), superoxide dismutase (SOD) assay, catalase (CAT) assay, lipid peroxidation (MDA) assay, gamma glutamyl transferase (GGT), glutathione peroxidase I (GPx1) assay, 5'-nucleotidase (CD73) activity assay, were procured from Abcam (Cambridge, USA).

Preparation of TQ-Entrapped Liposomes

TQ-entrapped DOPE/CHEMS comprising pH-sensitive stealth liposomes were prepared as described earlier.^{30,45,46} Briefly, the 6:4 ratio of DOPE: CHEMS in moles were mixed with 5% and 1% of mPEG-DSPE and TQ respectively in the solvents, and thin film was prepared using the rotary evaporator in N₂ environment. The unilamellar vesicles (ULVs) were achieved by the sonication of multilamellar vesicles (MLVs), following hydration of lipid film with the phosphate saline buffer. The ULVs were then passed through the decreasing pore-sized polycarbonate membranes from 400 to 100 nm several times with the help of handheld extruder at ambient temperature. Then, after centrifuging the liposomal solution for 25 minutes at 25,000 rpm, the supernatant was decanted to remove any untrapped TQ.

Characterization of Liposomes

The Entrapment Efficiency (EE), Zeta (ζ) Potential (mV) and Poly Dispersity Index (PDI), and Size of TQ Containing and Empty Liposomes

The UV spectrophotometer was used to evaluate the entrapment efficiency (EE) of TQ as described earlier.⁴⁷ The liposomes were lysed with 0.5% Triton-X-100 and the amount of TQ entrapped in the liposomes was calculated using the following formula.

$$\% \text{ Entrapment Efficiency (EE) of the drug} = \frac{\text{Liposome entrapped drug}}{\text{Total drug}} \times 100$$

The size, zeta potential as well as PDI of TQ-loaded and empty liposomes were evaluated by dynamic light scattering (DLS) in the Zetasizer Nano system (Malvern Instruments, Malvern, Worcestershire, UK) as described earlier.²⁸

In vitro Stability of Liposomes and Release Kinetics of TQ

The leakage of TQ in the PBS at 37 °C, as reported previously, was used to evaluate the stability of TQPSL.^{28,29} In brief, 1 mL of TQPSL was incubated in the dialysis bags (MWCO 3.5kDA), for 72 hours against 20 mL of 9% sucrose solution in PBS with continuous gentle shaking. At specific time points as 1, 2, 4, 8, 12, 18, 24, 36, 48, 60 and 72 hours, 1 mL of solution was withdrawn and substituted with 1 mL of PBS. After determining the quantity of TQ using a UV spectrophotometer, the release of TQ in the PBS was estimated using the formula given elsewhere.

The kinetics of TQ release from TQPSL in 90% bovine serum was studied at several time points ranging from 1 to 72 hours, as previously described.²⁹ Then, the mixture was withdrawn at each time point followed by centrifugation and estimation of TQ as stated above.

$$\text{TQ release(\%)} = \frac{C_n V + \sum_{i=0}^n C_i V_i}{w} \times 100\%$$

where C_n and C_i are the amounts of TQ in the mixture at the “ n ” and “ i ” sampling points, respectively, while V and V_i are the final mixture (20 mL) and collected sample (1mL) at each point, correspondingly.

pH-Dependent Leakage of TQ by TQPSL

The pH-responsive release kinetics of TQPSL was also assessed similarly as stated above with varying pH as pH-7.4, pH-6.5 and pH-5.5 as well.

In vivo Studies

Mice

All the female Swiss albino mice with the age of 8–10 weeks were purchased from the animal facility in the KSU, Riyadh, Saudi Arabia. All the animal experiments including the induction of lung cancer using chemical carcinogen, bleeding, injection, as well as the sacrifice of the mice were conducted following guidelines of the University of London Animal Welfare Society, Wheathampstead, England. The study protocol was approved by Animal Ethical Committee, Qassim University, Saudi Arabia, as cams1-2019-2-2-I-5538. All the experimental animals were housed in the animal facility of CAMS as per the guidelines and monitored throughout the study twice a day by well trained and dedicated staff members. All the surviving animals were euthanized by CO₂ inhalation at the end of the study following approved

procedure. However, the mice were also euthanized in a CO₂ chamber within 2–4 hours, whether they were moribund, or observed by a lack of sustained purposeful response to gentle stimuli. None of the mice died during the experiment before euthanasia.

Experimental Design

The 75 mice were randomly allocated into five groups, with each group consisting of 15 animals. The development of lung cancer by BaP, and sacrifice of animals were conducted as described earlier. The animals (5 mice/group) were sacrificed at the end of 22 weeks after the first exposure of BaP for further biochemical and histological analyses as described earlier.⁴⁸ The BaP, low dose TQPSL and high dose TQPSL were given 50 mg/kg, 20 mg/kg and 40 mg/kg body weight (b.w) respectively, through oral gavage, illustrated in detail in Figure 1. The survival of rest of the 10 mice in each group were monitored till 40 weeks. The mice were euthanized within 2–4 hours when they showed no response as stated above during the observational study, but reported dead in survival data.

Assessment of Survival Frequency, Body Weight and Relative Organ Weight

The survival of the animals was recorded till the end of 40 weeks following first dose of BaP. The body weight of each mouse were weighed at the start and monitored continuously every 2 weeks till the end of the experiment before sacrifice at the completion of week 22. The following formula was used to calculate the relative organ weight (ROW).

$$\text{ROW} = \frac{\text{Organ weight}}{\text{Body weight}} \times 100$$

Histopathological Analysis of Lung and Liver Tissues

The efficacy of TQPSL was analysed on the structural changes induced by BaP in the lungs and liver by histopathological analysis of the tissues using H&E staining. In short, the formalin-fixed tissues were processed, sectioned, and stained with hematoxylin and eosin (H&E) in a routine manner. The H&E staining of the tissues were studied under the light microscope at 100× and 400× magnifications with 100 μm and 50 μm scale bars, respectively.

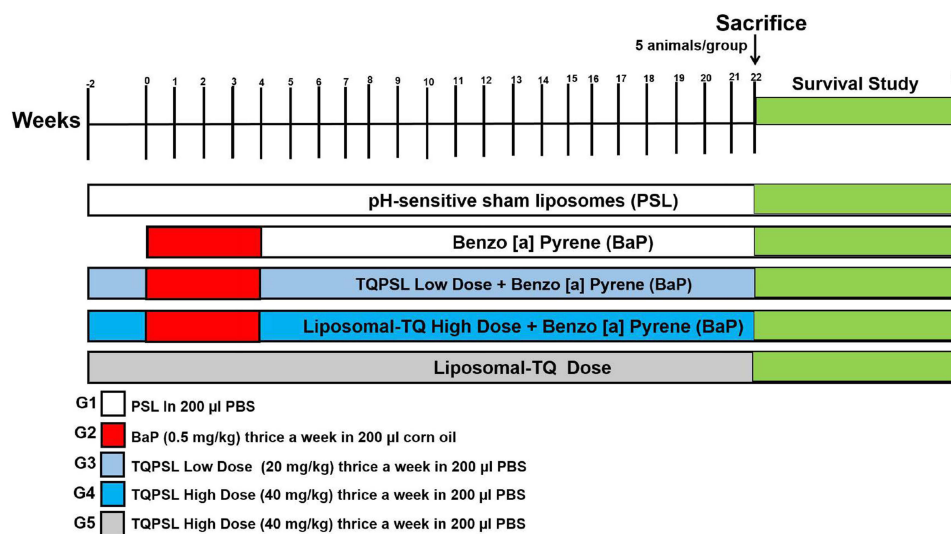


Figure 1 The schematic illustration of experimental design.

Notes: G1 (PSL in 200 μL PBS) thrice a week from -2 to week 21. G2 mice (50 mg/kg b.w in 200 mL corn oil) three times in a week from week 0 to week 4. G3 (low Dose TQPSL as 20 mg/kg) three times in a week from week -2 to week 21 + BaP as G2. G4 (high-dose TQPSL as 40 mg/kg) thrice a week from week -2 to week 21 + BaP as G2. G5 (high-dose TQPSL only) three times in a week from week 2 to week 21. The mice were given all the doses of BaP, PSL as well as TQPSL through oral gavage.

Abbreviations: BaP, benzo[a]pyrene; TQPSL, pH-sensitive liposomes of thymoquinone.

Serum Biochemical Analyses

Serum levels of carcinogenesis markers such as LDH, ADA, γ -GT, and 5'-NT were measured using Abcam kits as per the instructions given with the respective kits to determine the efficacy of TQPSL.

Antioxidant Enzyme Assays in Lung Tissues

The effect of various formulation on antioxidant enzymes was investigated as the activities of SOD, CAT, MDA and GPx1 in the lungs of all treated groups of animals. Briefly, the dissected pulmonary tissues were centrifuged in the buffer provided in kit of the respective enzymes and followed the manufacturer's instructions to determine the activity.

Annexin V-FITC/PI Apoptosis Assay

Flow cytometry was used to determine changes in cell distribution as viable, necrotic, and apoptotic (early and late) apoptotic phases. Briefly, the lung tissues from all treated group of animals were excised followed by the preparation of single-cell suspension using MACS tissue dissociator (Miltenyi Biotec, Germany). The cells were then filtered with 70 μ m mesh cell strainer and centrifuged at 300 g followed by suspending the cells in the binding buffer. The cells were stained with Annexin C-FITC and incubated for 30 minutes before being stained with propidium iodide, and the samples were analyzed using the MACS Analyzer 10 (Miltenyi Biotec, Germany). The analysis of the samples was conducted using FlowJo software v10.8.1.

Determination of Intracellular ROS Generation by Flow Cytometry

Flow cytometry was used to examine the formation of intracellular ROS using Abcam's DCFDA/H2DCFDA - Cellular ROS Assay Kit. Briefly, the cells were harvested as mentioned above and incubated with with 20 μ M of DCFDA for 30 minutes at 37°C, followed by the acquisition of samples in MACSQuant Analyzer 10. The changes in the generation of ROS were investigated using FlowJo software v10.8.1.

Molecular Docking Studies

The molecular docking approach was used to validate the interactions between TQ and numerous lung cancer therapeutic targets. The RCSB PDB database (<https://www.rcsb.org/>) was used to obtain the 3D structures of proteins mainly expressed by lung cancer genes. The PubChem database (<https://pubchem.ncbi.nlm.nih.gov/>) was used to retrieve the TQ's 3D structure in SDF format and translated to PDB format using the PyMol program (version 2.4). To add hydrogens, combine polar hydrogens, and compute charges of the ligand and protein receptors, M.G.L.Tools (version 1.5.7) software was utilized. In addition to examining the torsion root of the TQ molecule, the M.G.L.Tools were used to recognize the docking site in each protein. Following that, all of the protein and TQ were converted to pdbqt format. To execute molecular docking, AutoDock Vina 1.1.2 was used with an exhaustiveness value of 8 and the remainder of the settings left at their defaults.⁴⁹ After the docking experiment was completed successfully, the conformations of the bound TQ inside the target proteins were visualized using PyMol 2.5.1, LigPlot+ 2.4.2, and Biovia Discovery Studio Visualizer 2021 software, as previously described.^{50,51}

Statistical Analysis

The samples in different treated groups were compared by the mean values and standard errors. The significant differences between the treated groups were analysed by one-way and two-way ANOVA, Tukey's multiple comparison tests using Prism 9. P-value <0.05 was considered statistically significant.

Results

Characterization of Liposomes

Size, PDI, ζ Potential and EE

The DLS data revealed that the size of DOPE/CHEMS containing PEG-coated sham liposomes was found to be 115.5 nm with, whereas 128.7 nm was measured for TQPSL with <0.2 PDI homogeneity (Figure 2A). The ζ -potential of PSL and TQPSL was estimated as -15.9 and -19.5 mv, respectively, while the EE was calculated as 85% in TQPSL (Figure 2A).

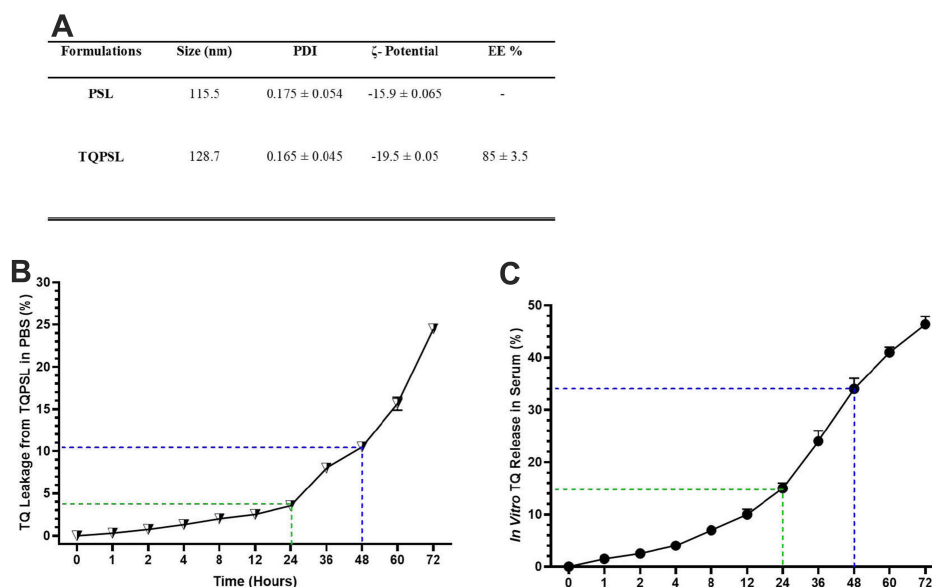


Figure 2 Characterization and in vitro stability and release kinetics of TQPSL.

Notes: (A) Size, PDI, ζ potential and EE, (B) stability of TQPSL in PBS, (C) release kinetics of TQ from TQPSL into the serum. The values are shown as SEM of three independent experiments.

Abbreviations: PDI, polydispersity index; EE, entrapment efficiency.

In vitro stability of liposomes and release kinetics of TQ

The results demonstrated the stability of TQPSL as only less than 5% and 11% TQ was estimated in the PBS at 37 °C after 24 and 48 hours respectively, while 25% was released after 72 hours (Figure 2B). The in vitro release kinetics data showed that less than 15%, 35% and 50% were measured in the serum after 24, 48 and 72 hours, correspondingly (Figure 2C).

pH-Responsiveness of TQPSL

The data revealed pH-dependent release of TQ as it was measured to be only 1% after the incubation of 8 hours at pH-7.4, while 12% and 29.7% were calculated at pH-6.5 and 5.5, respectively. As depicted in Figure S1, 50% (pH-5.5) and 28.2% (pH-6.5) TQ release were estimated, whereas only 2% at pH-7.4 after the incubation of TQPSL for 12 hours. The results demonstrated that 8% TQ was released at pH-7.4 after 30 hours, while 80% was estimated at pH-6.5. Interestingly, 100% TQ release was measured at pH-5.5 after the incubation of TQPSL for 30 hours (Figure S1).

In vivo Studies

Effect of TQPSL on BaP-Modulated Average Body Weight, Survival and ROW

The data showed significant reduction in the body weight of the animals exposed to BaP in G2 mice at the end of the experiment before survival as it was recorded to be 28.16 g, while 35.33 g was weighed in G1. However, the body weight was started increasing after 8 weeks but was not recovered completely due to the rapid fall during the week 6–8 as it decreased to 20.5 g in comparison to 26 g of G1 at week 8. The Kaplan–Meier curve revealed the 100% survival of the animals in TQPSL high dose (G4) pretreated mice, while 80% in TQPSL low doses (G3) after 40 weeks. The survival data also demonstrated the 60% mortality in the G2 group of animals exposed to BaP alone (Figure 3B). As depicted in Figure 3C and D, significant increase was measured as 1.0675 (69.7% relative to G1/G5) in the ROW of the mice exposed to BaP alone in G1 mice, while it was estimated as 0.67% in G1. The pretreatment of TQPSL showed the significant recovery in the ROW as it was calculated to be 0.85% and 0.7% in G3 and G3 groups of animals, respectively (Figure 3C and D).

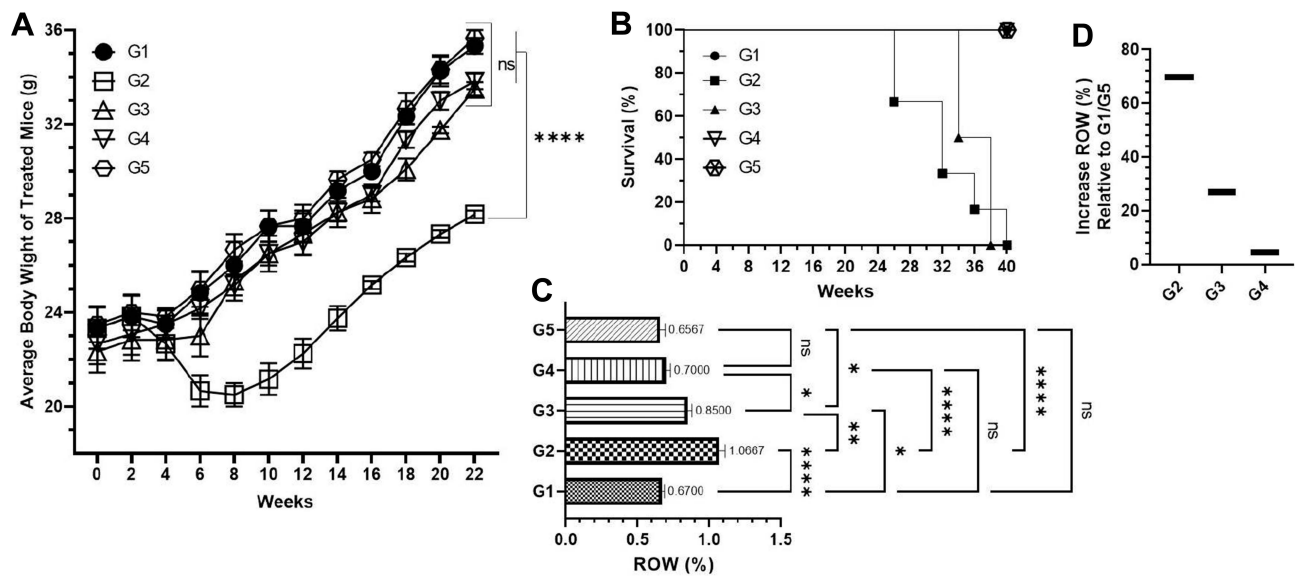


Figure 3 Effect of TQPSL on BaP-modulated average body weight, survival and ROW.

Notes: (A) Average body weight of the mice in different treated groups during the experiment. (B) Survival rate of the animals. (C) ROW. (D) Increased percentage of ROW relative to G1/G5. The values are shown as SEM of five mice in each group for (A and C), while 10 animals for (B). ^{NS}No Significance between the treated groups, *significant difference within the groups, p-value <0.05, **significant difference within the groups, p-value <0.01, ****significant difference within the groups, p-value <0.0001. **Abbreviation:** ROW, relative organ weight.

Effect of TQPSL on Cancer Marker Enzymes as ADA, AHH, GGT, 5-NT (CD73) and LDH in the Serum-Induced BaP

The modulation in the activities of cancer marker enzymes as ADA, AHH, GGT, 5-NT (CD73) and LDH was measured in the serum in all treated groups (Figure 4). The data revealed the significant increase in the activities of these enzymes by BaP in G2 as 3.4 μm (ADA), 1.66 μm (AHH), 2.0 μm (GGT), 2.73 μm (5-NT) and 1.927 (LDH) μm , while comparing G1 as 1.667 μm , 0.75 μm , 1.0 μm , 1.3 μm and 1.0 μm correspondingly (Figure 4A–E). As depicted in Figure 4A–E, the significant decline was noticed in activities of all the enzymes in the animals treated with TQPSL. The results demonstrated that 2.6 μm (G1) and 1.867 μm (G2), 1.25 μm (G1) and 0.9 μm (G2), 1.633 μm (G1) and 1.133 μm (G2), 1.96 μm (G1) and 1.4 μm (G2) and 1.51 μm (G1) and 1.18 μm (G2) were measured for ADA, AHH, GGT, 5-NT (CD73) and LDH, respectively (Figure 4A–E).

Effect of TQPSL on the Histopathology of Lungs and Liver

The histopathological data demonstrated the chemopreventive effect of TQPSL in the lung carcinoma and liver metastasis induced by BaP (Figure 5). The upper panel (UP) showed the 100x magnification with 100 μm scale bar, while lower panel (LP) revealed 400x magnification with 50 μm scale bar. As depicted in Figure 5A, alveolar damage and clusters of hyperchromatic cells (arrows in UP) having irregular nuclei and scant cytoplasm with adjacent bronchial and alveolar epithelial hyperplasia (arrow in LP) could be seen in G2, while G1 and G5 showed intact morphology of the lungs. In contrast, high dose of TQPSL (G4) exhibited preserved and near normal alveolar structures and respiratory bronchioles (arrow in LP), while G3 histology (arrows in UP and LP) revealed decreased alveolar injury and scanty scattered hyperchromatic cells (Figure 5A). The histopathological data exhibited distorted liver tissue architecture with clusters and clumps of metastatic small hyperchromatic cells (arrow in UP) having irregular nuclei and scanty cytoplasm (arrow in LP) in BaP alone exposed G2 mice (Figure 5B). The chemopreventive potential of TQPSL could be seen clearly as no sign of metastasis was observed in G3 and G4 as both showed the preserved tissue architecture (Figure 5B). However, focal presence of small clusters of small hyperchromatic cells beside the central vein (arrow) in G3 (arrows in UP & LP) and only few scattered inflammatory cells are noticed in G4 liver tissues (Figure 5B). The results also demonstrated the intact hepatocytes and sinusoids, surrounding the portal tract (arrows in UP & LP) in the G5 (Figure 5B).

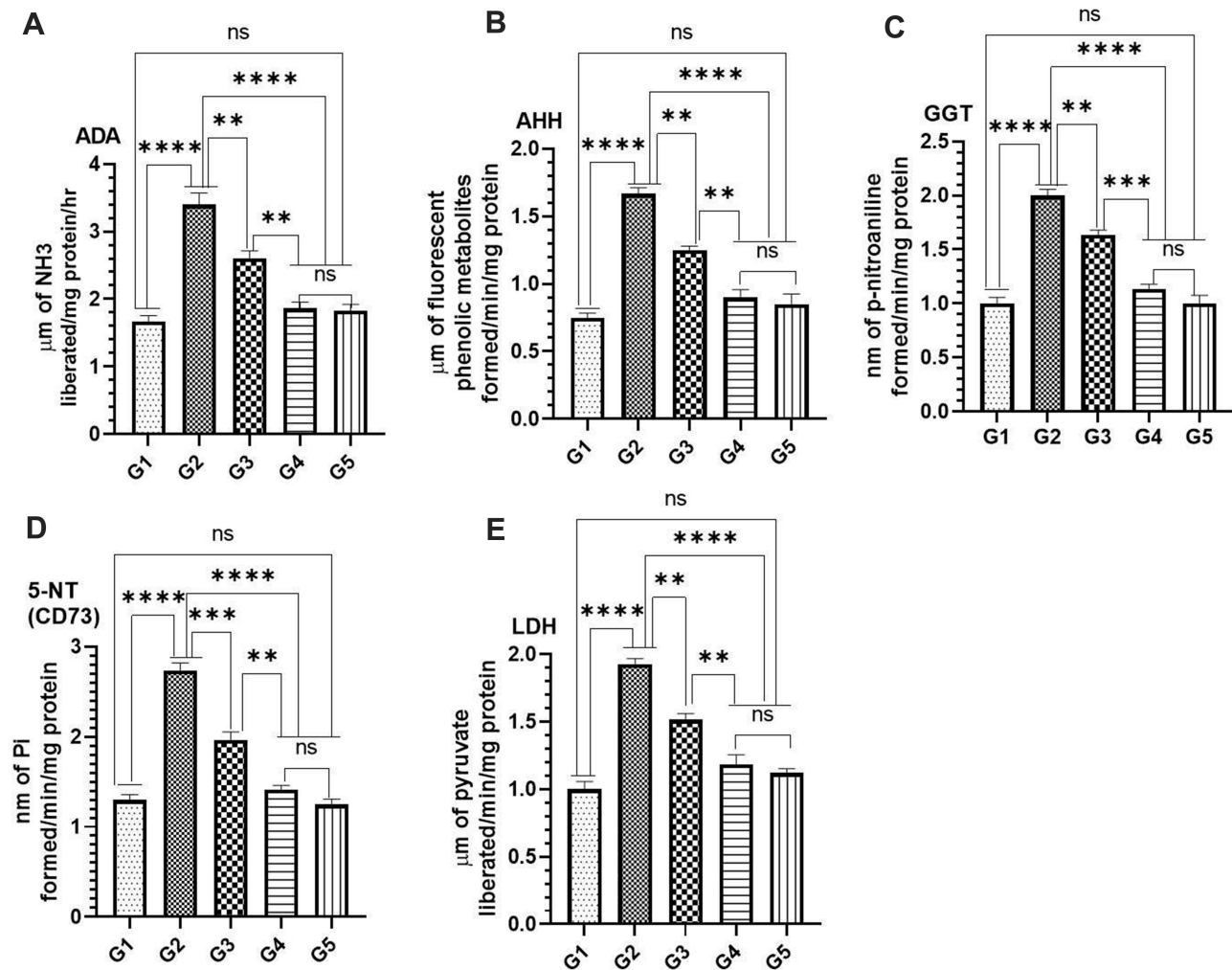


Figure 4 Effect of TQPSL on cancer marker enzymes in the serum.

Notes: (A) ADA, (B) AHH, (C) GGT, (D) 5-NT (CD73), (E) LDH. The values are shown as SEM of three independent experiments. ^{NS}No Significance between the treated groups, **significant difference within the groups, p-value <0.01, ***significant difference within the groups, p-value <0.001, ****significant difference within the groups, p-value <0.0001. **Abbreviations:** ADA, adenosine deaminase; AHH, aryl hydrocarbon hydroxylase; γ -GT, gamma glutamyl transferase; 5'-NT, 5'-nucleotidase; LDH, lactate dehydrogenase.

Effect of TQPSL on Antioxidant Enzymes as (A) SOD (B) CAT (C) MDA (D) GPx1 on BaP-Induced Small Cell Lung Carcinoma

The results showed significant reduction in the level of SOD, CAT and GPx1, while significant rise was seen in MDA in BaP exposed G2 mice (Figure 6). As depicted in Figure 6, the significant change was noticed to the normal level of these antioxidants in the mice pretreated with TQPSL. The data revealed that SOD increased to 4.063 units and 4.933 units, while its decreased to 2.133 units in G2, comparing 5.233 in G1 (Figure 6A). The level of CAT GPx1 and reduced to 93.33 units and 338.3 pg/mL in G2, respectively, while comparing 169.7 units and 793.3 pg/mL in G1 correspondingly. However, the TQPSL treated mice showed significant drop in the level of SOD, CAT and GPx1 as 4.063 units (G3) and 4.933 (G4), 127.3 μm (G3) and 156 μm (G4) and 513.3 pg/mL (G3) and 740 pg/mL (G4), respectively (Figure 6A, B and D). The level of MDA raised to 4.45 nm in G2, in comparison to 2.867 (G1) and 2.96 (G5), while its was measured as 3.7 nm and 3.1 nm in G3 and G4 correspondingly (Figure 6C).

Effect of TQPSL on the Induction of Apoptosis in the Lung Cells by Annexin V-FITC-PI Using Flow Cytometry in the Lungs

The apoptotic data exhibited the induction of early apoptosis in the animals treated with TQPSL (Figure 7). The FlowJo analysis of the samples showed 21.0% apoptotic cells in G3, while it was significantly increased to 33.8% in G4 (Figure 7). The data also demonstrated that no induction of apoptosis was measured in G1, G2 and G5 groups of animals (Figure 7).

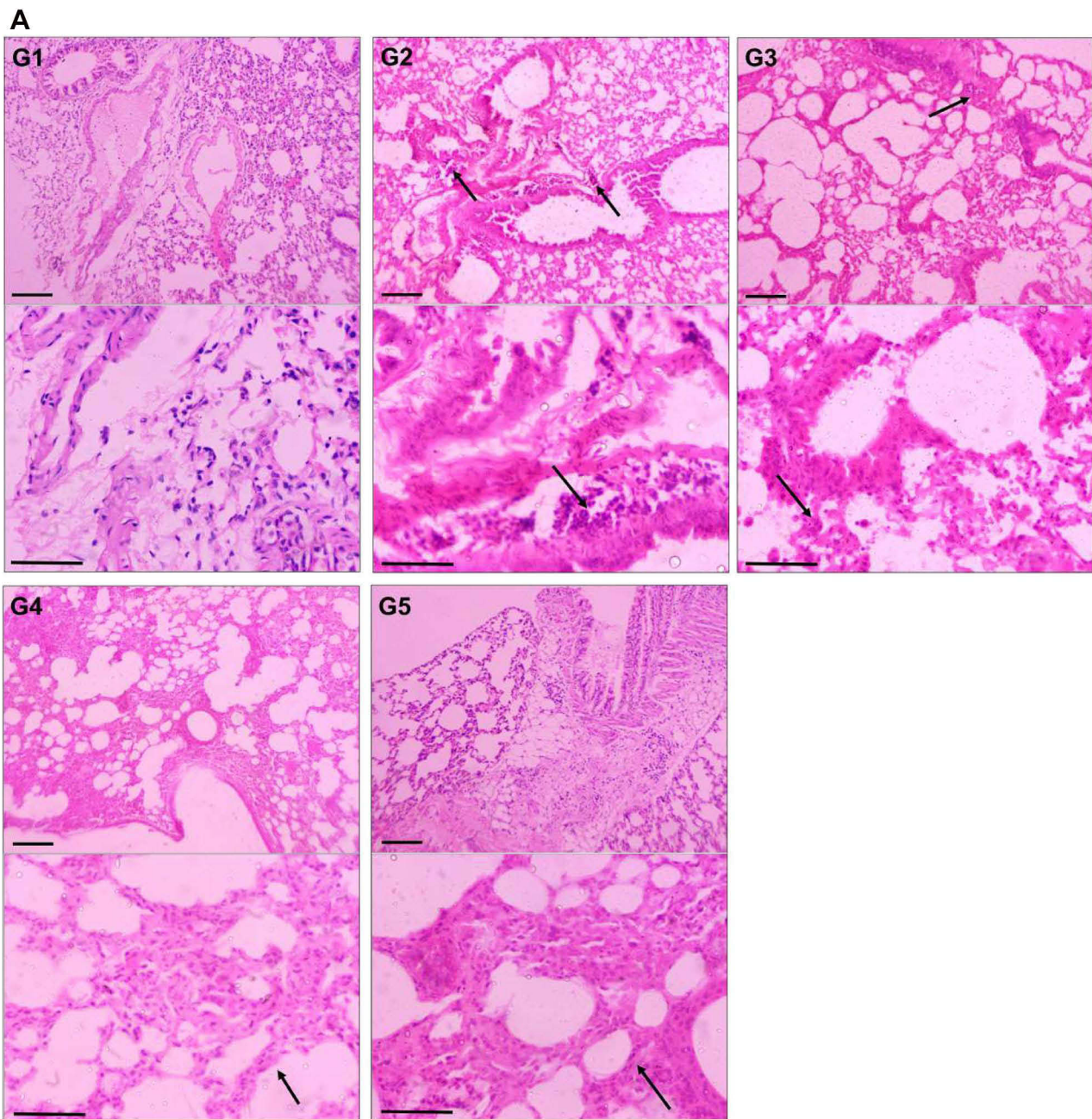


Figure 5 Continued.

Effect of TQPSL on the Generation of Intracellular ROS by DCFDA Using Flow Cytometry in the Lungs

The mean fluorescence intensity (MFI) of DCFDA was used to evaluate changes in intracellular ROS in lung cells from various treatment groups using flow cytometry. The data revealed that the significant induction of ROS was analyzed in the G2 group of animals exposed to BaP alone as 30,000 MFI, while only 3133 MFI was observed in G1. As depicted in [Figure 8](#), significant reduction in the ROS was noticed in TQPSL-treated G3 and G4 mice as it was recorded 9600 MFI and 3667 MFI, respectively ([Figure 8](#)).

Molecular Docking Studies

A molecular docking technique was used to evaluate the potential binding of TQ in the protein cavity of BRAF, RET, CDK7, mTOR, ALK, MLK4 kinase, MEK, and β -catenin exhibiting binding energy of -6.8 , -6.7 , -6.5 , 5.9 , 5.6 , -5.5 , -5.3 , and -4.2

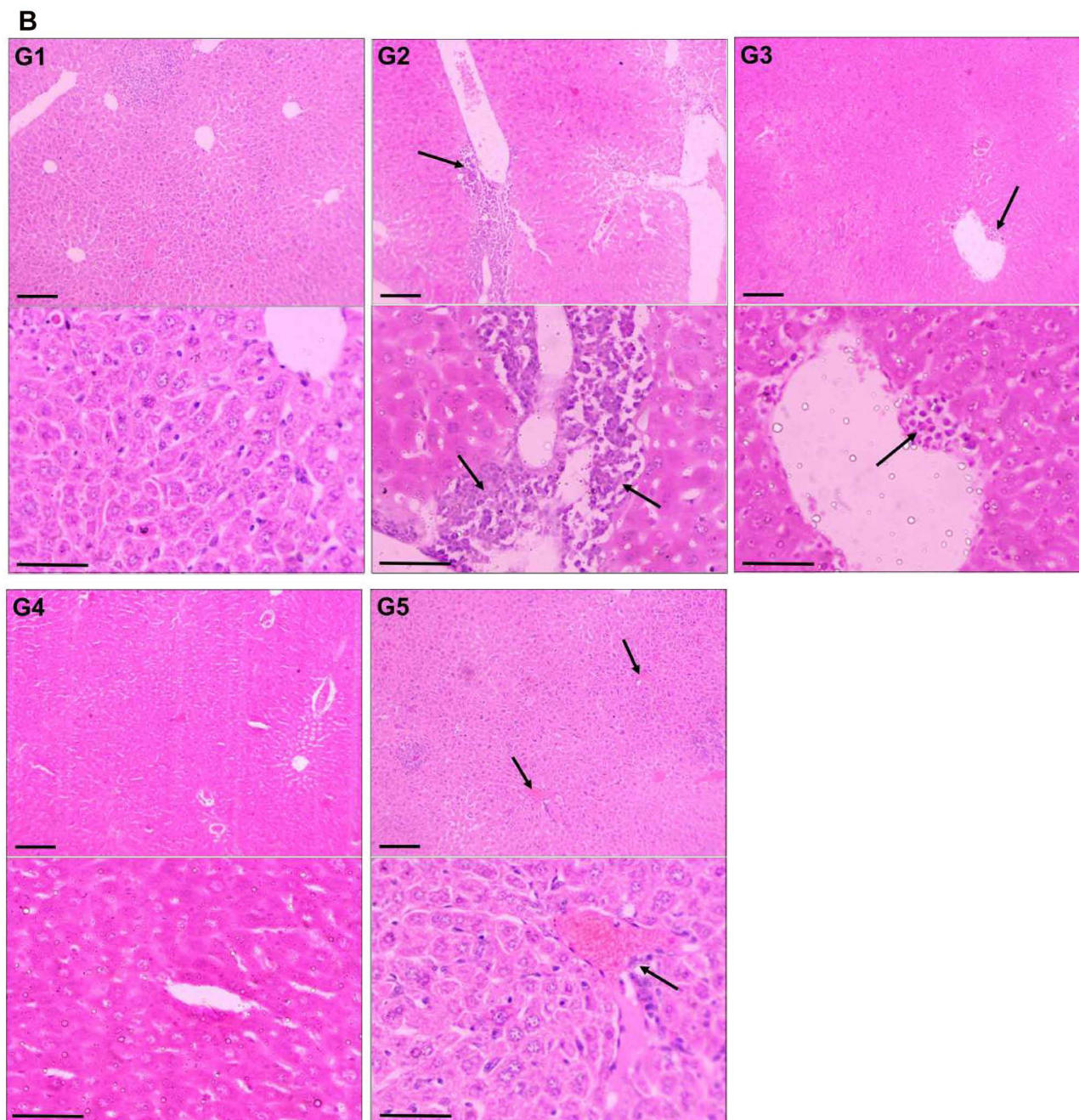


Figure 5 Effect of TQPSL on the histopathology of lungs and liver.

Notes: The representative H&E stained images of **(A)** Lungs. G1: Intact morphology. G2: approves the induction of small cell lung cancer, as alveolar damage and clusters of hyperchromatic cells having irregular nuclei and scant cytoplasm with adjacent bronchial and alveolar epithelial hyperplasia. G3: Decreased alveolar injury and scanty scattered hyperchromatic cells. G4: Largely preserved tissue structure as only few scattered inflammatory cells. G5: Normal morphology. **(B)** Liver. G1: Normal morphology. G2: Distorted tissue architecture with clusters and clumps of metastatic small hyperchromatic cells having irregular nuclei and scanty cytoplasm. G3: Preserved tissue architecture with focal presence of small cluster of small hyperchromatic cells beside the central vein. G4: Largely preserved tissue structure as only few scattered inflammatory cells. G5: Intact morphology. UP, 100× magnification, bar = 100 μm; LP, 400× magnification, bar = 50 μm.

Abbreviations: UP, upper panel; LP, lower panel.

kcal/mol, respectively (Table 1). The docking conformation that has maximum docking affinity score -6.8 kcal/mol represents great binding interactions between the TQ and BRAF protein, while minimum affinity was predicted against beta catenin showing -4.2 kcal/mol binding energy. Intermolecular interactions of docked TQ with serine/threonine-protein kinase B-raf

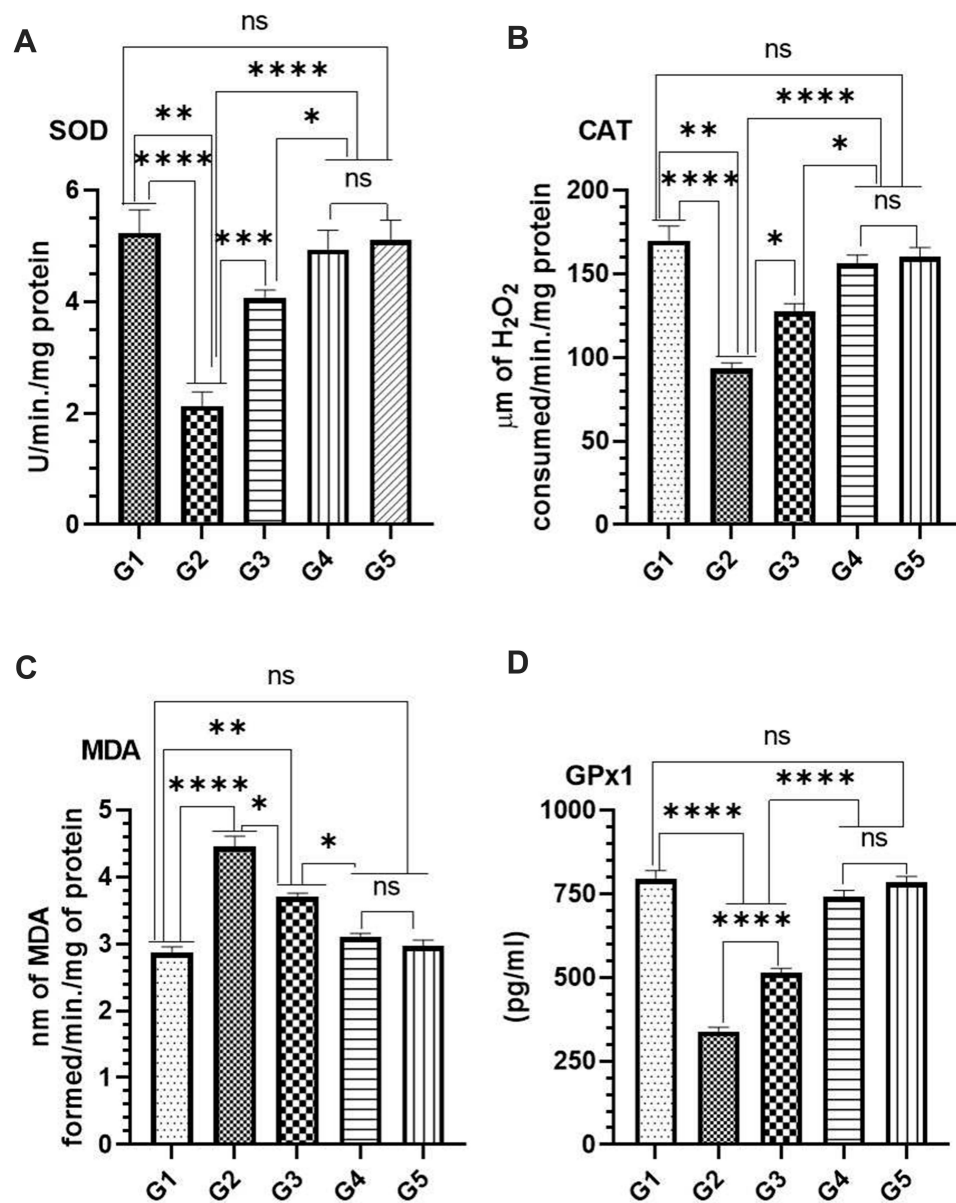


Figure 6 Effect of TQPSL on the level antioxidant enzymes in lung tissues.

Notes: (A) SOD, (B) CAT, (C) MAD, (D) GPx1. The values are shown as SEM of three independent experiments. ^{NS}No Significance between the treated groups, *significant difference within the groups, p-value <0.05, **significant difference within the groups, p-value <0.01, ***significant within the groups, p-value <0.001, ****significant difference within the groups, p-value <0.0001.

Abbreviations: SOD, superoxide dismutase; CAT, catalase; MDA, malondialdehyde dehydrogenase; GPx1, glutathione peroxidase I.

(BRAF) and rearranged during transfection (RET) kinase has been displayed in Figures 9 and 10, respectively. As presented in Figures 9 and 10, molecular interaction of the docked TQ involves both hydrophilic and hydrophobic types.

Discussions

The present study demonstrated the chemopreventive efficacy of PEG-coated pH-sensitive liposomes of TQ (TQPSL) in chemically induced lung cancer system in Swiss albino mice. This study is the first to establish the TQPSL, and characterized its entrapment efficiency, stability and release kinetics in the serum. The hydrophobic properties of TQ showed high EE as 85% in TQPSL with -19.5 mV ζ -potential. Recently, several strategies are focused on to the development of novel formulations of biologically active molecules for their cytoplasmic delivery to enhance the therapeutic efficacy. The formulation of pH-sensitive liposomes (PSLs) with a pH-mediated drug release strategy is a novel approach since they

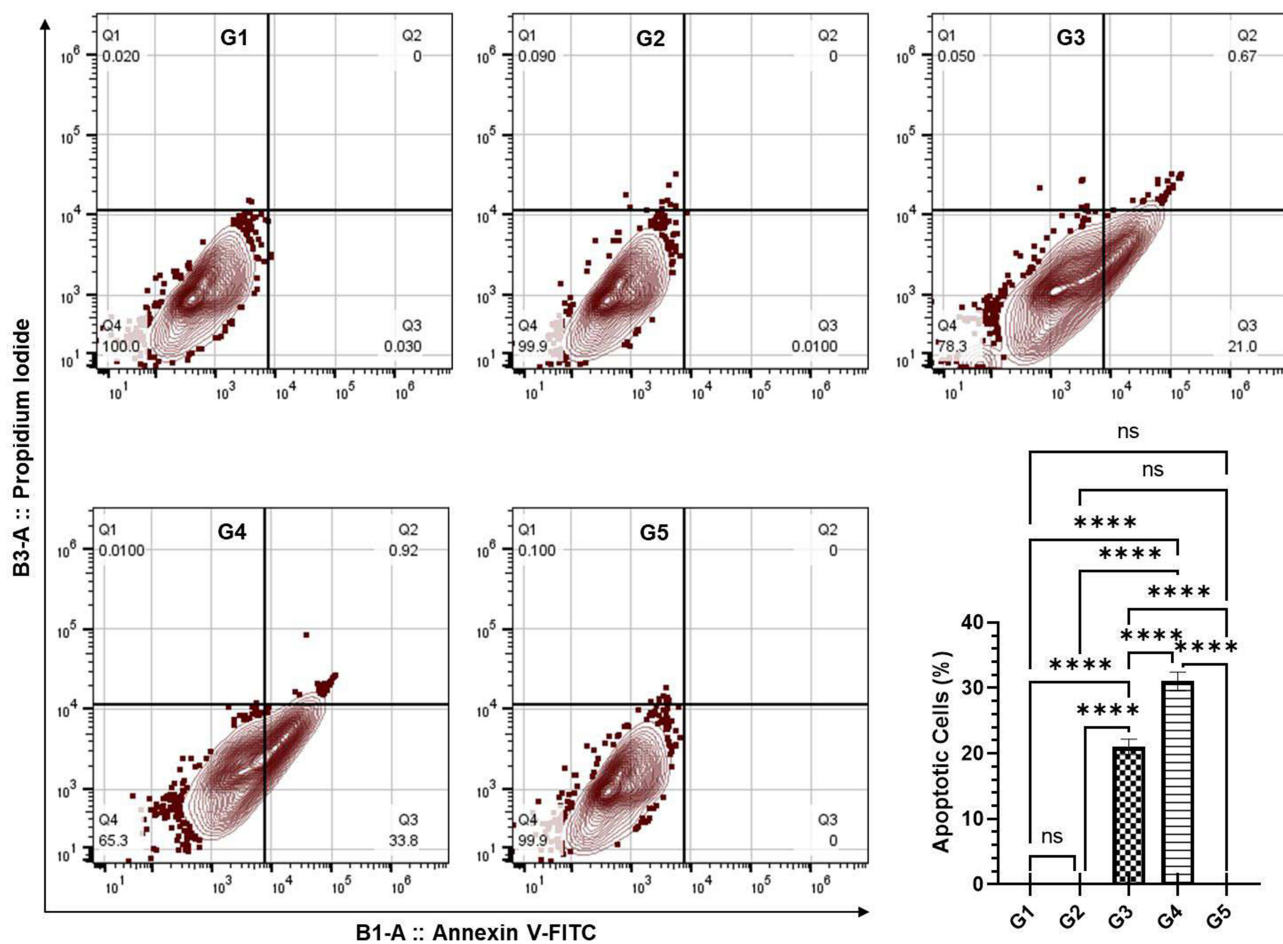


Figure 7 Effect of TQPSSL on the induction of apoptosis in the lung cells by Annexin V-FITC-PI using flow cytometry in the lungs.

Notes: The values are shown as SEM of three independent experiments. ^{NS}No Significance between the treated groups, ****significant difference within the groups, p-value <0.0001.

Abbreviations: FITC, fluorescein isothiocyanate; PI, propidium iodide.

destabilize and develop fusogenic features at slightly acidic pH, resulting in the release of their contents. Due to the acidic pH of endosomes, the entrapped medicament in the PSLs is released into the cytoplasm after penetration into the cells via endocytosis. Besides, the acidic pH of the tumor microenvironment and the delivery of entrapped drug in the PSLs also increase the delivery of it into the cytoplasm. Liposomes are stable because of the rigidity of lipid bilayers, which is dependent on the lipids used and their molar content, as well as an elevated phase transition temperature (T_c).^{52–55} The preparation of DOPE/CHEMS containing pH-sensitive liposomes are considered the most effective vehicle as the DOPE played the critical role in the destabilization of PSLs upon acidification. Following the lipids' acquisition of hexagonal inverted phase in the acidic environment, the entrapped medicaments in the PSLs are released into the cytoplasm. In addition, the inclusion of CHEMS with DOPE provides the required stability to the PSLs. As evident from various studies, the 6:4 molar ratio of DOPE and CHEMS has been demonstrated as most suitable, to make the liposomes highly stable and efficient.^{28,45,56–58} Despite their excellent stability, liposome clearance across RES is the major hurdle in developing novel delivery systems that target extra RES tissues. The inclusion of PEGylated lipids on the upper surface of liposomes improves their circulation time and delivers the entrapped drug/s on to the target site.^{59–61} The in vitro release data of TQPSSL demonstrated its great stability and prolong circulation as 24.5% and 46.33% TQ were measured in the PBS and serum respectively at 37 °C after 72 hours (Figure 2A and B). The hydrophobic nature of TQ also might be associated with slow release as it attaches sturdily to the lipids. Earlier investigations have also demonstrated a low concentration of TQ release due to the compound's hydrophobic character.^{30,62}

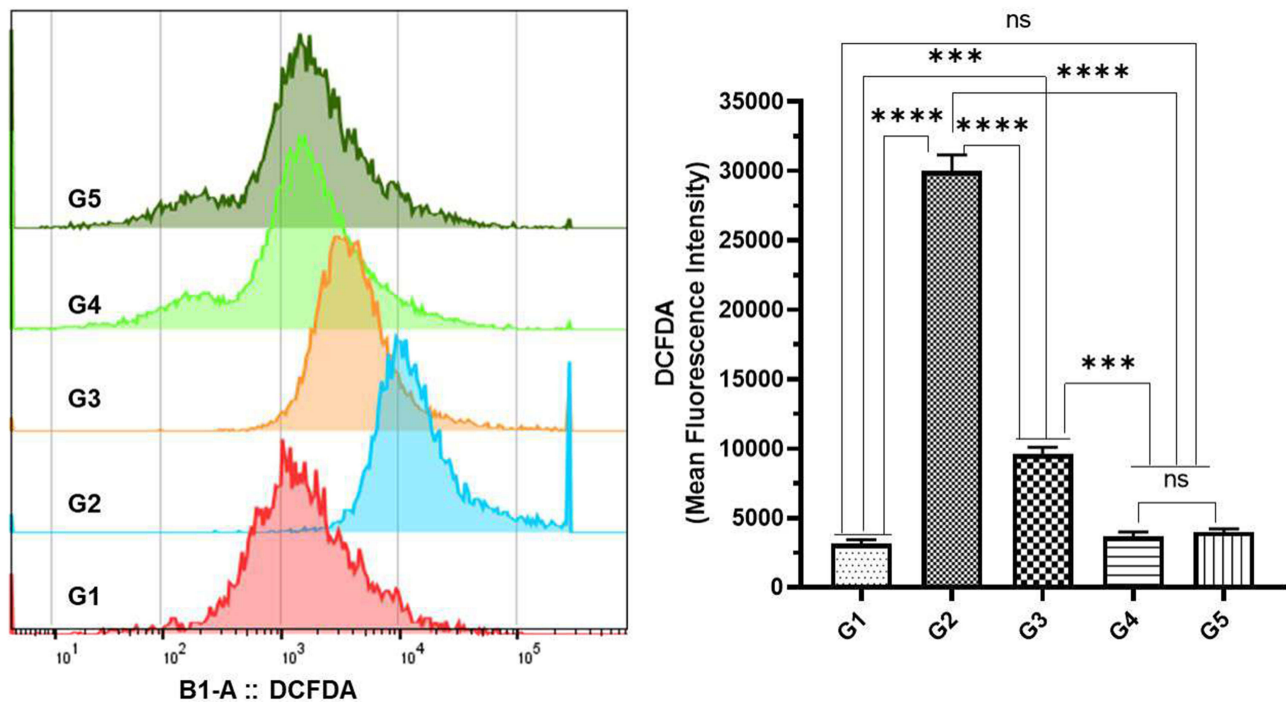


Figure 8 Effect of TQPSL on BaP-induced intracellular ROS by DCFDA using flow cytometry in the lungs.

Notes: The cellular ROS was estimated as MFI of DCFDA in the lung cells from the tissues of the animals treated with various formulations. The values are shown as SEM of three independent experiments. ^{NS}No Significance between the treated groups, ^{***}significant difference within the groups, p-value <0.001, ^{****}significant difference within the groups, p-value <0.0001.

Abbreviations: DCFDA, 2',7'-dichlorofluorescein diacetate; ROS, reactive oxygen species; MFI, mean fluorescent index.

A considerable decline in body weight was seen in G1 mice treated with BaP alone for 6–8 weeks, as shown in Figure 3A, due to cancer cachexia, as proven by multiple investigations.^{63,64} However, the treatment of TQPSL protected the mice from cancer cachexia condition as normal growth was observed in G3 and G4 mice throughout the study. Several studies have revealed that the lungs are enlarged due to inflammatory cell overload and the continuing proliferation of malignant cells.^{48,65} The data revealed that ~70% ROW was increased in G2 in comparison to G1/G5, while no significant change was measured in G4. However, G3 mice showed 26.8% increase in ROW while comparing G1/G5, but significant decrease on G2.

The increased activities of cancer marker enzymes in the serum are the important biomarkers to diagnose the stage of chemically induced carcinogenesis.^{66–69} The significant drop in the activities of AHH, γ -GT, 5'-NT, ADA, and LDH in the serum by TQPSL high dose clearly indicated its role in the delay in initiation, while TQPSL low dose protected the

Table I AutoDock Vina Results of TQ with Potential Anticancer Drug Targets

S. N.	Targets	PDB Code	Binding Energy of TQ (kcal/mol)
1	Serine/threonine-protein kinase B-raf (BRAF)	6P7G	-6.8
2	Rearranged during transfection (RET) kinase	6VHG	-6.7
3	Cyclin-dependent kinase-7	1UA2	-6.5
4	Mammalian target of rapamycin (mTOR)	4JT6	-5.9
5	Anaplastic lymphoma kinase (ALK)	4CNH	-5.6
6	Mixed-lineage kinase 4 (MLK4)	4UYA	-5.5
7	MAPK/ERK kinase (MEK)	7JUV	-5.3
8	Beta catenin	3SL9	-4.2

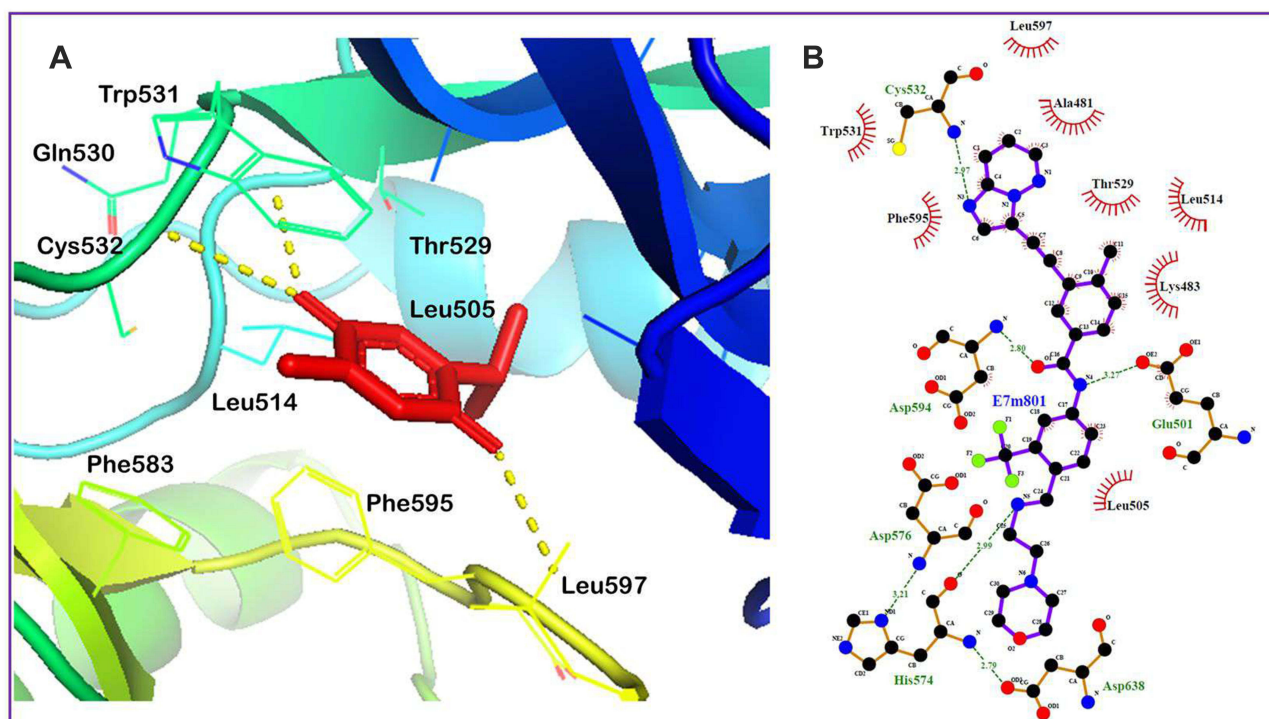


Figure 9 (A) Minimum energy conformation of the docked thymoquinone (shown as red sticks) in the binding pocket of BRAF protein showing hydrogen bond interaction as yellow lines. (B) Co-crystallized inhibitor of the BRAF protein (PDB ID: 6P7G), 3-[(imidazo[1,2-b]pyridazin-3-yl)ethynyl]-4-methyl-N-[4-({[2-(morpholin-4-yl)ethyl]amino)methyl}-3-(trifluoromethyl)phenyl]benzamide, occupying the binding site.

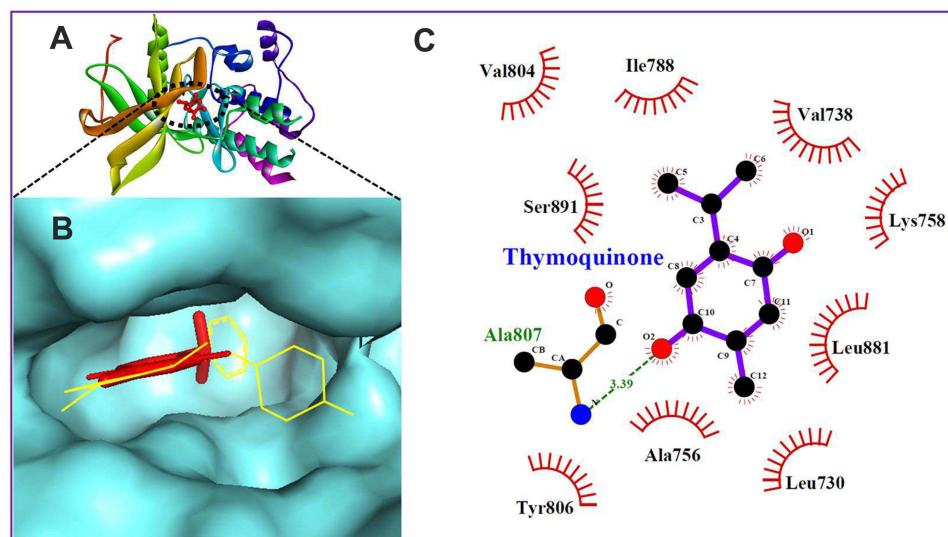


Figure 10 (A and B) Docking conformation TQ in the RET protein (shown as ribbon and surface style in (A and B), respectively). Superimposition of the docked TQ (shown as red stick) and native co-crystallized inhibitor of the RET protein (shown as yellow line in (B)). (C) LigPlot diagram of the docked TQ.

lungs in the promotion as well as progression of lung cancer (Figure 4). The results also showed the protection of liver metastasis in the mice treated with TQPSL (Figure 5).

The induction of high level of ROS plays an important role in the process of chemically induced carcinogenesis as the lungs are exposed directly to the environmental pollutants.^{70–72} Our results demonstrated the potential of TQPSL as it significantly

protected the release of lipid peroxidation products, such as MDA (Figure 6). Furthermore, TQPSL showed the delay in the progression of cancer in the lungs by preventing ROS accumulation, which was confirmed by histopathological studies (Figures 5 and 8). Several antioxidant enzymes play the crucial role in the scavenging of free radicals in ROS-induced oxidative damage. The increased activities of SOD and CAT prevent the cells from ROS-induced oxidative damage by scavenging free radicals. Mainly, the superoxide anions and lipid peroxidation-induced oxidative stress are prevented by SOD, while the CAT plays the major role in the breakdown of H₂O₂ in cancer cells.^{73,74} Several researchers showed the significant decrease in the activity of these enzymes in the rodents by BaP.^{75–78} Our results clearly demonstrated the significant revival of antioxidant enzymes such as GPx1, SOD and CAT in the mice continuously exposed to TQPSL in G3 and G4, which were measured significantly low in BaP-exposed G2 mice, while comparing G1 and G5 (Figure 6). Furthermore, the evaluation of apoptotic cells shows the potential of the drugs in the removal of abnormal cell through programmed cell death.^{79,80} The flow cytometry data revealed the induction of apoptosis in the G3 and G4 mice treated with TQPSL to maintain the tissue homeostasis in the lungs by inhibiting damaged or abnormal cells (Figure 7).

Although liposomes are intriguing carriers for the delivery of drugs to treat a range of illnesses, including cancer, the active component only interacts with enzymes, receptors, signal transduction proteins, and other targets to elicit pharmacological actions. In this regard, the molecular docking technique is frequently employed to elucidate the interaction mechanism of therapeutic compounds encapsulated in liposomal formulations.^{81,82} Therefore, molecular docking study was performed with various pharmacological targets that are important for anticancer drug development to understand the predictive foundation for possible TQ interactions. To the best of our knowledge, this is the first research to use molecular docking to define the compound's molecular interactions with the pharmacological targets linked with lung cancer. TQ displayed the maximum affinity for the BRAF protein and the lowest affinity for the beta catenin in this in silico study. The BRAF protein is crystallized with the inhibitor, 3-[(imidazo[1,2-*b*] pyridazin-3-yl)ethynyl]-4-methyl-*N*-[4-({[2-(morpholin-4-yl) ethyl] amino} methyl)-3-(trifluoromethyl)phenyl]benzamide surrounded by the amino acids such as Ala481, Lys483, Glu501, Leu505, Leu514, Thr529, Trp531, Cys532, His574, Asp576, Asp594, Phe595, Leu597, and Asp638, providing a binding site for molecular docking. TQ binds to the ligand binding site of BRAF and stabilized itself by forming hydrogen bonds with Gln530, Cys532 and Leu597. This suggests that potential binding of TQ with the ligand binding site of BRAF and might be involved in inhibition of BRAF activity, leading to its anticancer effect. TQPSL has been shown to have chemopreventive properties in mice with chemically induced small cell lung cancer in mice. Furthermore, the in-silico study identified many therapeutic targets of TQ that should be further investigated in lung cancer in vitro and in vivo models.

Conclusions

In the present study, we developed the PEG coated long circulating, pH-sensitive liposomes of TQ (TQPSL). The results summarize the chemopreventive profile of TQPSL in BaP-induced lung cancer animal model. The pre-treatment of TQPSL not only protected the liver metastasis, but also prevented the promotion and progression of cancer in the lungs. This is the first study in the development of TQ formulations, considering low solubility of TQ and pulmonary delivery challenges as well. In order to fully comprehend the molecular mechanism of TQPSL in the treatment of lung cancer, more research is needed, concentrating on the molecular targets of TQ suggested by molecular docking studies.

Acknowledgements

The authors gratefully acknowledge the Deanship of Scientific Research, Qassim University, Buraydah, Saudi Arabia, for the financial support for this research under the Grant # cams1-2019-2-2-I-5538 during the academic year 2019.

Disclosure

The authors report no conflicts of interest for this work.

References

1. Sung H, Ferlay J, Siegel RL, et al. Global cancer statistics 2020: GLOBOCAN estimates of incidence and mortality worldwide for 36 cancers in 185 countries. *CA Cancer J Clin.* 2021;71:209–249. doi:10.3322/caac.21660
2. Ruppert A-M, Amrioui F, Fallet V. [Risk factors and prevention of lung cancer]. *Rev Prat.* 2020;70:852–856. French.

3. McFarland DC. A response to “Psychological symptoms and survival in patients with metastatic lung cancer: smoking must be the first concern!”. *Psycho Oncol.* 2020;29:1504–1505. doi:10.1002/pon.5405
4. Sasco AJ, Secretan MB, Straif K. Tobacco smoking and cancer: a brief review of recent epidemiological evidence. *Lung Cancer.* 2004;45:S3–S9. doi:10.1016/j.lungcan.2004.07.998
5. Shen H, Spitz MR, Qiao Y, et al. Smoking, DNA repair capacity and risk of nonsmall cell lung cancer. *Int J Cancer.* 2003;107:84–88. doi:10.1002/ijc.11346
6. Zou X, Fu Y, Wu D, Liu J, Xiao Y, Huang H. [Establishment of mouse lung cancer model induced by benzo[a]pyrene dynamic inhalation exposure]. *Wei Sheng Yan Jiu.* 2020;49:486–490. Chinese.
7. Ceppi M, Munnia A, Cellai F, Bruzzone M, Peluso MEM. Linking the generation of DNA adducts to lung cancer. *Toxicology.* 2017;390:160–166. doi:10.1016/j.tox.2017.09.011
8. Osborne MR, Brookes P, Beland FA, Harvey RG. The reaction of (\pm)-7 α , 8 β -dihydroxy-9 β , 10 β -epoxy-7,8,9,10-tetrahydrobenzo(a)pyrene with DNA. *Int J Cancer.* 1976;18:362–368. doi:10.1002/ijc.2910180315
9. Pucci C, Martinelli C, Ciofani G. Innovative approaches for cancer treatment: current perspectives and new challenges. *EcancerMedicalscience.* 2019;13. doi:10.3332/ecancer.2019.961
10. Charmsaz S, Prencipe M, Kiely M, Pidgeon G, Collins D. Innovative technologies changing cancer treatment. *Cancers.* 2018;10:208. doi:10.3390/cancers10060208
11. Hameed R, Khan A, Khan S, Perveen S. Computational approaches towards kinases as attractive targets for anticancer drug discovery and development. *Anticancer Agents Med Chem.* 2019;19:592–598. doi:10.2174/1871520618666181009163014
12. Thomford N, Senthilane D, Rowe A, et al. Natural products for drug discovery in the 21st century: innovations for novel drug discovery. *Int J Mol Sci.* 2018;19:1578. doi:10.3390/ijms19061578
13. Wolfender J-L, Litaudon M, Touboul D, Queiroz EF. Innovative omics-based approaches for prioritisation and targeted isolation of natural products – new strategies for drug discovery. *Nat Prod Rep.* 2019;36:855–868. doi:10.1039/C9NP00004F
14. Chopra B, Dhingra AK. Natural products: a lead for drug discovery and development. *Phytother Res.* 2021;35:4660–4702. doi:10.1002/ptr.7099
15. Patra S, Pradhan B, Nayak R, et al. Dietary polyphenols in chemoprevention and synergistic effect in cancer: clinical evidences and molecular mechanisms of action. *Phytomedicine.* 2021;90:153554. doi:10.1016/j.phymed.2021.153554
16. Ma L, Zhang M, Zhao R, Wang D, Ma Y, Li A. Plant natural products: promising resources for cancer chemoprevention. *Molecules.* 2021;27:26. doi:10.3390/molecules26040933
17. Newman DJ, Cragg GM. Natural products as sources of new drugs over the nearly four decades from 01/1981 to 09/2019. *J Nat Prod.* 2020;83:770–803. doi:10.1021/acs.jnatprod.9b01285
18. de Kok TM, van Breda SG, Manson MM. Mechanisms of combined action of different chemopreventive dietary compounds: a review. *Eur J Nutr.* 2008;47(Suppl 2):51–59. doi:10.1007/s00394-008-2006-y
19. Malik S, Singh A, Negi P, Kapoor VK. Thymoquinone: a small molecule from nature with high therapeutic potential. *Drug Discov Today.* 2021;26:2716–2725. doi:10.1016/j.drudis.2021.07.013
20. Gali-Muhtasib H, Roessner A, Schneider-Stock R. Thymoquinone: a promising anti-cancer drug from natural sources. *Int J Biochem Cell Biol.* 2006;38:1249–1253. doi:10.1016/j.biocel.2005.10.009
21. Khan MA, Younus H. Thymoquinone shows the diverse therapeutic actions by modulating multiple cell signaling pathways: single drug for multiple targets. *Curr Pharm Biotechnol.* 2018;19:934–945. doi:10.2174/1389201019666181113122009
22. Khader M, Eckl PM. Thymoquinone: an emerging natural drug with a wide range of medical applications. *Iran J Basic Med Sci.* 2014;17:950–957.
23. Botnick I, Xue W, Bar E, et al. Distribution of primary and specialized metabolites in *Nigella sativa* seeds, a spice with vast traditional and historical uses. *Molecules.* 2012;17:10159–10177. doi:10.3390/molecules170910159
24. Ansary J, Giampieri F, Forbes-Hernandez TY, et al. Nutritional value and preventive role of *Nigella sativa* L. and its main component thymoquinone in cancer: an evidenced-based review of preclinical and clinical studies. *Molecules.* 2021;26:2108. doi:10.3390/molecules26082108
25. Asaduzzaman khan M, Tania M, Fu S, Fu J. Thymoquinone, as an anticancer molecule: from basic research to clinical investigation. *Oncotarget.* 2017;8:51907–51919. doi:10.18632/oncotarget.17206
26. Rathore C, Rathbone MJ, Chellappan DK, et al. Nanocarriers: more than tour de force for thymoquinone. *Expert Opin Drug Deliv.* 2020;17:479–494. doi:10.1080/17425247.2020.1730808
27. Salmani J, Asghar S, Lv H, Zhou J. Aqueous solubility and degradation kinetics of the phytochemical anticancer thymoquinone; probing the effects of solvents, pH and light. *Molecules.* 2014;19:5925–5939. doi:10.3390/molecules19055925
28. Khan A, Alsahli MA, Aljasir MA, et al. Safety, stability, and therapeutic efficacy of long-circulating TQ-incorporated liposomes: implication in the treatment of lung cancer. *Pharmaceutics.* 2022;14:153. doi:10.3390/pharmaceutics14010153
29. Allemailem KS, Alnuqaydan AM, Almatroudi A, et al. Safety and therapeutic efficacy of thymoquinone-loaded liposomes against drug-sensitive and drug-resistant *Acinetobacter baumannii*. *Pharmaceutics.* 2021;14:13. doi:10.3390/pharmaceutics13050677
30. Khan MA, Aljarbou AN, Khan A, Younus H. Liposomal thymoquinone effectively combats fluconazole-resistant *Candida albicans* in a murine model. *Int J Biol Macromol.* 2015;76:203–208. doi:10.1016/j.ijbiomac.2015.02.015
31. Odeh F, Ismail SI, Abu-Dahab R, Mahmoud IS, Al Bawab A. Thymoquinone in liposomes: a study of loading efficiency and biological activity towards breast cancer. *Drug Deliv.* 2012;19:371–377. doi:10.3109/10717544.2012.727500
32. Odeh F, Naffa R, Azzam H, et al. Co-encapsulation of thymoquinone with docetaxel enhances the encapsulation efficiency into PEGylated liposomes and the chemosensitivity of MCF7 breast cancer cells to docetaxel. *Heliyon.* 2019;5:e02919. doi:10.1016/j.heliyon.2019.e02919
33. Patel HM, Ryman BE. Oral administration of insulin by encapsulation within liposomes. *FEBS Lett.* 1976;62:60–63. doi:10.1016/0014-5793(76)80016-6
34. Khan I, Gothwal A, Sharma AK, Qayum A, Singh SK, Gupta U. Biodegradable nano-architectural PEGylated approach for the improved stability and anticancer efficacy of bendamustine. *Int J Biol Macromol.* 2016;92:1242–1251. doi:10.1016/j.ijbiomac.2016.08.004
35. Minato S, Iwanaga K, Kakemi M, Yamashita S, Oku N. Application of polyethyleneglycol (PEG)-modified liposomes for oral vaccine: effect of lipid dose on systemic and mucosal immunity. *J Control Release.* 2003;89:189–197. doi:10.1016/s0168-3659(03)00093-2

36. Gabizon A, Papahadjopoulos D. Liposome formulations with prolonged circulation time in blood and enhanced uptake by tumors. *Proc Natl Acad Sci.* 1988;85:6949–6953. doi:10.1073/pnas.85.18.6949
37. Slepishkin V, Simões S, de Lima MCP, Düzgüneş N. Sterically stabilized pH-sensitive liposomes. *Methods Enzymol.* 2004;387:134–147. doi:10.1016/S0076-6879(04)87008-3
38. Woodle MC, Lasic DD. Sterically stabilized liposomes. *Biochim Biophys Acta.* 1992;1113:171–199. doi:10.1016/0304-4157(92)90038-c
39. Shahraiki N, Mehrabian A, Amiri-Darban S, Moosavian SA, Jaafari MR. Preparation and characterization of PEGylated liposomal Doxorubicin targeted with leptin-derived peptide and evaluation of their anti-tumor effects, in vitro and in vivo in mice bearing C26 colon carcinoma. *Colloids Surf B Biointerfaces.* 2021;200:111589. doi:10.1016/j.colsurfb.2021.111589
40. Mozar FS, Chowdhury EH. Impact of PEGylated nanoparticles on tumor targeted drug delivery. *Curr Pharm Des.* 2018;24:3283–3296. doi:10.2174/1381612824666180730161721
41. Pozzi D, Colapicchioni V, Caracciolo G, et al. Effect of polyethyleneglycol (PEG) chain length on the bio-nano-interactions between PEGylated lipid nanoparticles and biological fluids: from nanostructure to uptake in cancer cells. *Nanoscale.* 2014;6:2782–2792. doi:10.1039/c3nr05559k
42. Chow T-H, Lin -Y-Y, Hwang -J-J, et al. Improvement of biodistribution and therapeutic index via increase of polyethylene glycol on drug-carrying liposomes in an HT-29/luc xenografted mouse model. *Anticancer Res.* 2009;29:2111–2120.
43. Pang X, Jiang Y, Xiao Q, Leung AW, Hua H, Xu C. pH-responsive polymer-drug conjugates: design and progress. *J Control Release.* 2016;222:116–129. doi:10.1016/j.jconrel.2015.12.024
44. Shi J, Kantoff PW, Wooster R, Farokhzad OC. Cancer nanomedicine: progress, challenges and opportunities. *Nat Rev Cancer.* 2017;17:20–37. doi:10.1038/nrc.2016.108
45. Khan A, Aljarbou AN, Aldebasi YH, et al. Fatty acid synthase (FASN) siRNA-encapsulated-Her-2 targeted fab³-immunoliposomes for gene silencing in breast cancer cells. *Int J Nanomedicine.* 2020;15:5575–5589. doi:10.2147/IJN.S256022
46. Khan A, Aljarbou AN, Khan S, Khan MA. Her-2-directed systemic delivery of fatty acid synthase (FASN) siRNA with novel liposomal carrier systems in the breast cancer mouse model. *J Drug Target.* 2022;1–12. doi:10.1080/1061186X.2022.2038613
47. Khan MA, Aldebasi YH, Alsuhaibani SA, et al. Therapeutic potential of thymoquinone liposomes against the systemic infection of *Candida albicans* in diabetic mice. *PLoS One.* 2018;13:e0208951. doi:10.1371/journal.pone.0208951
48. Khan A, Alhumaydhi FA, Alwashmi AS, et al. Diallyl sulfide-mediated modulation of the fatty acid synthase (FASN) leads to cancer cell death in BaP-induced lung carcinogenesis in Swiss mice. *J Inflamm Res.* 2020;13:1075–1087. doi:10.2147/JIR.S284279
49. Trott O, Olson AJ. AutoDock Vina: improving the speed and accuracy of docking with a new scoring function, efficient optimization, and multithreading. *J Comput Chem.* 2010;31:455–461. doi:10.1002/jcc.21334
50. Fahmy NM, Al-Sayed E, Moghannem S, Azam F, El-Shazly M, Singab AN. Breaking down the barriers to a natural antiviral agent: antiviral activity and molecular docking of *Erythrina speciosa* extract, fractions, and the major compound. *Chem Biodivers.* 2020;17:e1900511–e1900511. doi:10.1002/cbdv.201900511
51. Azam F. Elucidation of teicoplanin interactions with drug targets related to COVID-19. *Antibiotics.* 2021;10:856. doi:10.3390/antibiotics10070856
52. Li M, Du C, Guo N, et al. Composition design and medical application of liposomes. *Eur J Med Chem.* 2019;164:640–653. doi:10.1016/j.ejmech.2019.01.007
53. Ahmed KS, Hussein SA, Ali AH, Korma SA, Lipeng Q, Jinghua C. Liposome: composition, characterisation, preparation, and recent innovation in clinical applications. *J Drug Target.* 2019;27:742–761. doi:10.1080/1061186X.2018.1527337
54. Anderson M, Omri A. The effect of different lipid components on the in vitro stability and release kinetics of liposome formulations. *Drug Deliv.* 2004;11:33–39. doi:10.1080/10717540490265243
55. Crommelin DJ. Influence of lipid composition and ionic strength on the physical stability of liposomes. *J Pharm Sci.* 1984;73:1559–1563. doi:10.1002/jps.2600731118
56. Briuglia M-L, Rotella C, McFarlane A, Lamprou DA. Influence of cholesterol on liposome stability and on in vitro drug release. *Drug Deliv Transl Res.* 2015;5:231–242. doi:10.1007/s13346-015-0220-8
57. Magarkar A, Dhawan V, Kallinteri P, et al. Cholesterol level affects surface charge of lipid membranes in saline solution. *Sci Rep.* 2014;4:5005. doi:10.1038/srep05005
58. Papahadjopoulos D, Cowden M, Kimelberg H. Role of cholesterol in membranes. Effects on phospholipid-protein interactions, membrane permeability and enzymatic activity. *Biochim Biophys Acta.* 1973;330:8–26. doi:10.1016/0005-2736(73)90280-0
59. Vargason AM, Anselmo AC, Mitragotri S. The evolution of commercial drug delivery technologies. *Nature Biomed Eng.* 2021;5:951–967. doi:10.1038/s41551-021-00698-w
60. Singh A, Neupane YR, Shafi S, Mangla B, Kohli K. PEGylated liposomes as an emerging therapeutic platform for oral nanomedicine in cancer therapy: in vitro and in vivo assessment. *J Mol Liq.* 2020;303:112649. doi:10.1016/j.molliq.2020.112649
61. Jiménez-López J, Bravo-Caparrós I, Cabeza L, et al. Paclitaxel antitumor effect improvement in lung cancer and prevention of the painful neuropathy using large pegylated cationic liposomes. *Biomed Pharmacother.* 2021;133:111059. doi:10.1016/j.biopha.2020.111059
62. Mostafa M, Alaaeldin E, Aly UF, Sarhan HA. Optimization and characterization of thymoquinone-loaded liposomes with enhanced topical anti-inflammatory activity. *AAPS PharmSciTech.* 2018;19:3490–3500. doi:10.1208/s12249-018-1166-1
63. Pain VM, Randall DP, Garlick PJ. Protein synthesis in liver and skeletal muscle of mice bearing an ascites tumor. *Cancer Res.* 1984;44:1054–1057.
64. Petruzzelli M, Wagner EF. Mechanisms of metabolic dysfunction in cancer-associated cachexia. *Genes Dev.* 2016;30:489–501. doi:10.1101/gad.276733.115
65. Greten FR, Grivnenkov SI. Inflammation and cancer: triggers, mechanisms, and consequences. *Immunity.* 2019;51:27–41. doi:10.1016/j.immuni.2019.06.025
66. Sadeck N, Ibrahim BM, Alassal MA. Cytochrome P450-isoenzyme 1A1 in susceptibility to tobacco-related lung cancer. *Asian Cardiovasc Thorac Ann.* 2014;22:315–318. doi:10.1177/0218492313492987
67. Miao P, Sheng S, Sun X, Liu J, Huang G. Lactate dehydrogenase a in cancer: a promising target for diagnosis and therapy. *IUBMB Life.* 2013;65:904–910. doi:10.1002/iub.1216
68. Xie H, Hanai J, Ren J-G, et al. Targeting lactate dehydrogenase-A inhibits tumorigenesis and tumor progression in mouse models of lung cancer and impacts tumor-initiating cells. *Cell Metab.* 2014;19:795–809. doi:10.1016/j.cmet.2014.03.003

69. Nikkhoo B, Sigari N, Ghaderi B, et al. Diagnostic utility of adenosine deaminase in serum and bronchoalveolar lavage fluid for screening lung cancer in Western Iran. *J Med Biochem*. 2013;32:109–115. doi:10.2478/jomb-2013-0011
70. Nicco C, Laurent A, Chereau C, Weill B, Batteux F. Differential modulation of normal and tumor cell proliferation by reactive oxygen species. *Biomed Pharmacother*. 2005;59:169–174. doi:10.1016/j.biopha.2005.03.009
71. Reuter S, Gupta SC, Chaturvedi MM, Aggarwal BB. Oxidative stress, inflammation, and cancer: how are they linked? *Free Radic Biol Med*. 2010;49:1603–1616. doi:10.1016/j.freeradbiomed.2010.09.006
72. Shadel GS, Horvath TL. Mitochondrial ROS signaling in organismal homeostasis. *Cell*. 2015;163:560–569. doi:10.1016/j.cell.2015.10.001
73. Forman HJ, Zhang H. Targeting oxidative stress in disease: promise and limitations of antioxidant therapy. *Nat Rev Drug Discov*. 2021;20:689–709. doi:10.1038/s41573-021-00233-1
74. Pham-Huy LA, He H, Pham-Huy C. Free radicals, antioxidants in disease and health. *Int J Biomed Sci*. 2008;4:89–96.
75. Oyewole AO, Birch-Machin MA. Mitochondria-targeted antioxidants. *FASEB J*. 2015;29:4766–4771. doi:10.1096/fj.15-275404
76. Bodduluru LN, Kasala ER, Madhana RM, et al. Naringenin ameliorates inflammation and cell proliferation in benzo(a)pyrene induced pulmonary carcinogenesis by modulating CYP1A1, NFκB and PCNA expression. *Int Immunopharmacol*. 2016;30:102–110. doi:10.1016/j.intimp.2015.11.036
77. Kasala ER, Bodduluru LN, Barua CC, Gogoi R. Antioxidant and antitumor efficacy of Luteolin, a dietary flavone on benzo(a)pyrene-induced experimental lung carcinogenesis. *Biomed Pharmacother*. 2016;82:568–577. doi:10.1016/j.biopha.2016.05.042
78. Hudlikar RR, Pai V, Kumar R, et al. Dose-related modulatory effects of Polymeric Black Tea Polyphenols (PBPs) on initiation and promotion events in B(a)P and NNK-induced lung carcinogenesis. *Nutr Cancer*. 2019;71:508–523. doi:10.1080/01635581.2019.1578389
79. Kaufmann SH, Earnshaw WC. Induction of apoptosis by cancer chemotherapy. *Exp Cell Res*. 2000;256:42–49. doi:10.1006/excr.2000.4838
80. Kerr JF, Wyllie AH, Currie AR. Apoptosis: a basic biological phenomenon with wide-ranging implications in tissue kinetics. *Br J Cancer*. 1972;26:239–257. doi:10.1038/bjc.1972.33
81. Refaat H, Mady FM, Sarhan HA, Rateb HS, Alaeldin E. Optimization and evaluation of propolis liposomes as a promising therapeutic approach for COVID-19. *Int J Pharm*. 2021;592:120028. doi:10.1016/j.ijpharm.2020.120028
82. Baldi A, Chaudhary M, Sethi S, Abhiav Chandra R, Madan J, Madan J. Armamentarium of nanoscaled lipid drug delivery systems customized for oral administration: in silico docking patronage, absorption phenomenon, preclinical status, clinical status and future prospects. *Colloids Surf B Biointerfaces*. 2018;170:637–647. doi:10.1016/j.colsurfb.2018.06.061

Journal of Inflammation Research

Dovepress

Publish your work in this journal

The Journal of Inflammation Research is an international, peer-reviewed open-access journal that welcomes laboratory and clinical findings on the molecular basis, cell biology and pharmacology of inflammation including original research, reviews, symposium reports, hypothesis formation and commentaries on: acute/chronic inflammation; mediators of inflammation; cellular processes; molecular mechanisms; pharmacology and novel anti-inflammatory drugs; clinical conditions involving inflammation. The manuscript management system is completely online and includes a very quick and fair peer-review system. Visit <http://www.dovepress.com/testimonials.php> to read real quotes from published authors.

Submit your manuscript here: <https://www.dovepress.com/journal-of-inflammation-research-journal>